Chapter 4

Seismic Attenuation Problem

Problem Presented By: Kenneth J. Hedlin (Husky Energy); Gary Margrave (University of Calgary)

Mentors: Nilima Nigam (McGill University); Tobias Schaefer (University of North Carolina at Chapel Hill)

Student Participants: Mohammad al-Khaleel (McGill); Linping Dong and Carlos Montana (University of Calgary); Wan Chen, Catherine Dupuis, Gilles Hennenfend, Felix Hermann and Peyman Poor Moghaddam (University of British Columbia); Heejeong Lee and Jinwoo Lee (Seoul National University); Joohee Lee (University of North Carolina at Chapel Hill); Namyong Lee (Minnesota State University); Yan Wu (University of Manitoba)

Report prepared by: Nilima Nigam (nigam@math.mcgill.ca)

4.1 Introduction

Seismic imaging, a technique in which the reflections of a source seismic wave are recorded as it passes through the earth, is a major tool for geophysical exploration. Seismic imaging can be used to reconstruct a profile of the material properties of the earth below the surface, and is thus widely used for locating hydrocarbons.

The problem presented by Husky Energy concerns seismic attenuation: the loss of energy as a seismic wave propagates through the earth. As an exploration tool, attenuation effects have only recently attracted attention. These effects can prove useful in two ways: as a means of correcting seismic data to enhance resolution of standard imaging techniques, and as a direct hydrocarbon indicator. Theoretically, a subsurface reservoir full of hydrocarbons will tend to be acoustically softer than a porous rock filled only with water; Kumar et al show that attenuation is highest in a partially fluid-saturated rock.

Many physical processes can lead to the attenuation of a seismic trace. In the present work, we ignore attenuation effects such as spherical divergence or scattering, and concentrate on intrinsic attenuation effects exclusively. The latter are caused by friction, particularly in porous rocks between fluid and solid particles, see [2, 7].

The goal of the workshop was to find a means of computing seismic attenuation from relatively short windows of seismic imaging data, and particularly be able to identify regions of anomalous attenuation.

The paper is organised as follows. We begin by a detailed description of the attenuation problem in Section 4.2, collecting important notation and assumptions for easy reference. The reader may find the simple numerical example presented in Section 4.2.3 useful to fix ideas.

In Section 4.3, we consider the use of *frequency-shift techniques* to identify anomalous attenuation; two different attributes are used on simulated and real data. In Section 4.4, different wavelet-based denoising techniques are used to identify the attenuation anomaly. In Section 4.5, we present the mathematical ideas behind an extension of a Wiener technique. We end the paper in Section 4.6 with ideas for future work, including the use of a constrained optimization problem for estimating the attenuation.

4.2 Problem Statement

The ability of a material to attenuate seismic waves is measured by a dimensionless quantity Q, called the *attenuation factor*, by

$$Q := \frac{\text{energy of seismic wave}}{\text{energy dissipated per cycle of wave}} = \frac{2\pi E}{\triangle E}$$

where E is the energy of the wave, and $\triangle E$ is the change in energy per cycle. Typical values of Q range from 5-20 (dirt) through 100 (rock) to 10,000 (steel). In what follows, we assume that this attenuation factor is independent of frequency ω in the useful seismic bandwidth. The attenuation of the wave is directly linked to the different layers that compose the Earth, so that whenever changes in the composition of layers occur, the attenuation changes too. This is why we would like to be able to detect changes in attenuation, as it would enable us to identify s change material properties.

Goal: *To estimate Q from given seismic data.*

In this paper, we restrict our attention to 1-D models, in which all geological layers are horizontal. In addition, we assume the source and receiver are effectively coincident. We assume that the receiver is positioned at the surface of the earth (in other words, we do not consider vertical seismic profiles).

For a medium with linear stress-strain relation, it is known that wave amplitude A is proportional to $\sqrt{E}$. Hence,

$$\frac{1}{Q} = -\frac{\Delta A}{\pi A} \tag{4.1}$$

from which we can obtain the amplitude fluctuations due to attenuation. That is, given initial amplitude A_0, let λ be the wave length given in terms of frequency ω and phase velocity c by $\lambda = 2\pi c/\omega$, then $\Delta A = \lambda(dA/dz)$. Hence, equation (4.1) becomes,

$$\frac{dA}{dz} = -\frac{\omega}{2cQ}A \tag{4.2}$$

with the exponential decaying solution

$$A(\omega, z) = A_0(\omega) \exp\left(-\frac{\omega z}{2cQ}\right). \tag{4.3}$$

Now, from observation of exponentially decaying values of $A(\omega, z)$, we can compute Q value. That is, from (4.3), we have

$$\ln\left(\frac{A}{A_0}\right) = -\omega\left(\frac{z}{2cQ}\right) = -\omega\left(\frac{t}{2Q}\right) \tag{4.4}$$

Here we assume that the phase velocity c does not depend on frequency, ie, that there are no dispersion effects. This has the added effect of correlating well the time of travel of the reflected wave with the depth of the layer from which the reflection occurs.

Hence, by recording the $\ln(A/A_0)$ versus ω graph, and then estimate the *average* slope, we can recover the value of Q. This idea is known as *log spectral ratio* method.

Another model, which includes the effect of reflections of the signal from various layers, is as follows. Let $s_k(t)$ denote the seismic trace obtained from layer k, received at time t_k at the receiver (assuming the source signal s_0 was emitted at time $t = 0$). Suppose the coefficient of reflection at the kth layer is r_k, and the the source signal is s_o. In general, r_k is unknown, as is s_o. Indeed, the source signal is usually generated by a denotation; characterizing this signal is not possible.

In the Fourier domain at frequency ω, we may write

$$|\hat{s}_k(\omega)| = r_k|\hat{s}_o(\omega)|e^{-p\omega t/Q} \tag{4.5}$$

where p is a constant, and r_k is the coefficient of reflectivity of the kth layer.

Suppose we have similar information about a seismic trace reflected from layer j, then the log spectral ratio method estimates the attenuation Q as:

$$\log\left(\frac{|\hat{s_k}|}{|\hat{s_j}|}\right) = \log|r_k| - \log|r_j| + \frac{p\omega}{Q}(t_j - t_k).$$

4.2.1 A Convolutional Model of Attenuation

Let $s(t)$ denote an unattenuated seismic trace received at time t at a receiver. If $w(t)$ was the source waveform and $r(t)$ is the reflectivity as a function of depth (equivalently time), then we may write

$$s(t) = w * r := \int_{-\infty}^{\infty} w(\tau) r(t - \tau)\, d\tau. \tag{4.6}$$

Two key assumptions are made regarding the source signal and the reflectivity:

- *the white reflectivity assumption*. The white reflectivity assumption simply means the reflectivity r satisfies

  $$\int_{-\infty}^{\infty} \tilde{r}(s) r(t - s)\, ds = \delta(t)$$

  where $\delta(t)$ is the Dirac measure.

- *the minimum phase assumption*: this means that the source signal $w(t)$ is causal, invertible, and possesses minimum phase in the sense that if we write the signal in the frequency domain

$$\hat{w}(\omega) = A_0(\omega)e^{i\phi(\omega)}$$

we can find the phase $\phi(\omega)$ by using a Hilbert transform.

With these assumptions, and in the absence of attenuation, we are able to recover the source signal w from a given trace s using the Wiener process on equation (4.6):

$$s * \tilde{s} = (w * r) * (\tilde{w} * \tilde{r}) = (w * \tilde{w}) * \delta.$$

Taking a Fourier transform of the above expression, we get the amplitude $A(\omega)$ of the source signal w; the minimum phase assumption now allows us to recover the phase.

Unfortunately, the Wiener process does not apply in quite such a straight-forward fashion to the case where the signal is attenuated. The process of attenuation is described by the action of a pseudo differential operator: the attenuated trace s_a is now

$$s_a(t) := \int_{-\infty}^{\infty} w_\alpha(\tau, t-\tau)r(\tau)d\tau \tag{4.7}$$

where

$$w_\alpha(u;v) := \int_{-\infty}^{\infty} \alpha(u,\eta)e^{i\eta v}\hat{w}(\eta)\, d\eta, \tag{4.8}$$

$$\alpha(u,\eta) = \exp\left(-\frac{\eta u}{2Q}\right)\exp\left(\frac{iu}{2Q}\int_{-\infty}^{\infty}\frac{e}{\eta - e}\, de\right). \tag{4.9}$$

In Section 4.5 we describe an extension of the Wiener technique to the case of attenuated waves.

We can also describe, in the setting of this convolutional model, the windowed log spectral ratio technique which is commonly used. Let Ω_1 and Ω_2 be two intervals of time over which the seismic trace s_a has been sampled. We expect that

$$\hat{s_a}(\Omega_1) \approx \hat{w}_{\text{eff}_1} \cdot \hat{r}_{\text{eff}_1}$$

where w_{eff_1} is the effective signal over window Ω_1, and r_{eff_1} is the effective reflectivity and the hats denote the Fourier transform.

We also expect that

$$|\hat{w}_{\text{eff}_2}| = |\hat{w}_{\text{eff}_1}|\exp(-\frac{\omega\Delta\tau}{2Q})$$

where $\Delta\tau$ is the window separation. Therefore, the log spectral ratio is

$$\log\left(\frac{|\hat{s}_a(\Omega_1)|}{|\hat{s}_a(\Omega_2)|}\right) = \frac{\omega\Delta\tau}{2Q} + \log\left(\frac{|\hat{r}_{\text{eff}_1}|}{|\hat{r}_{\text{eff}_2}|}\right).$$

4.2.2 A Discrete Model

In practice, seismic trace data is sampled at discrete time intervals, for a finite duration of time. We therefore describe a discrete version of the convolutional model above: suppose we know the initial source signal, as well as the attenuation and reflectivity properties of the medium being sampled. Let the data be sampled at times $t_1, t_2, \ldots t_n$. From this, we can construct a matrix W_α, and a vector of reflectivities $\boldsymbol{r} = (r_1, r_2, \ldots r_n)^T$, where r_i is the reflectivity of the layer at depth ct_i. Then, the discrete version of equation (4.7) is

$$W_\alpha \boldsymbol{r} = (\boldsymbol{w_1}|\boldsymbol{w_2}|\ldots|\boldsymbol{w_n})\,\boldsymbol{r} = \boldsymbol{s} := (s_1, s_2, \ldots s_n)^T.$$

The entries w_{ij} of matrix W_α have the following properties:

- If $t_i > t_j$, $w_{ji} = 0$ (causality assumption)
- If $t_i < t_j$, $w_{ji} = w_\alpha(t_i, t_j - t_i)$, where w_α was defined by equations (4.8) and (4.9).

Therefore, W_α is lower triangular, and the amplitude spectra of column vectors $\boldsymbol{w}_i$ attenuate by an exponential factor from left to right.

The *forward seismic problem* is: given W_α, $\boldsymbol{r}$, find the seismic trace vector $\boldsymbol{s}$.

The *inverse seismic problem* is: given $\boldsymbol{s}$, find W_α, $\boldsymbol{r}$. In our specific case, we have to find W_α, specifically the amount of attenuation between the amplitude spectra of the columns of W_α. As is easy to see, the inverse problem is quite ill-posed.

4.2.3 A Simple Model

As a first approach to solving the attenuation retrieval problem, we began by creating some simulated data and solving the forward problem, where the Q-profile is known. The intermediate goal is to see how the presence of the anomaly changes a known signal.

The data is sampled for $t = 2$ s, at intervals of time 0.002 s. The seismic trace vector $\boldsymbol{s}$ thus has 1000 entries. The reflectivity vector $\boldsymbol{r}$ is drawn from a nearly-white probability distribution. The source signal w has dominant frequency 20 Hz, is generated once, and used repeatedly.

We consider the following simple 1-D models as shown in the picture Figure 4.1(a):

- The normal attenuation case, where the attenuation is a constant $Q = 100$ for all depths;
- The anomalous attenuation case, where Q changes at depth $ct = 1$ to $Q = 40$, and then changes back to $Q = 100$ at depth $ct = 1.1$ (we assume the speed of propagation has been normalized to $c = 1$).

We calculate the resultant seismic traces $s(t)$ as it propagates through the two media. In Figure 4.1(b) we show the computed seismic traces with and without the anomaly. As can be seen, the two traces appear nearly identical; only when we subtract them can we clearly spot the onset of the anomaly (at time $t = 1$).

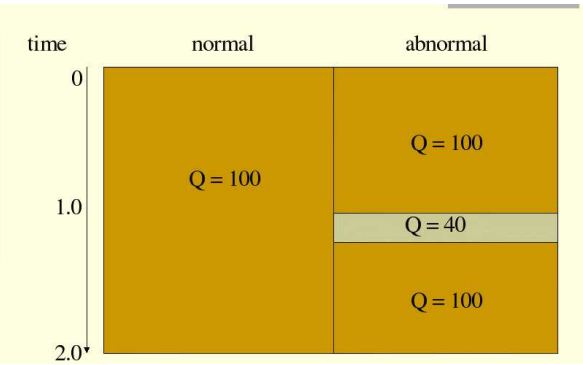

(a) Profile of "normal" and "anomalous" attenuation.

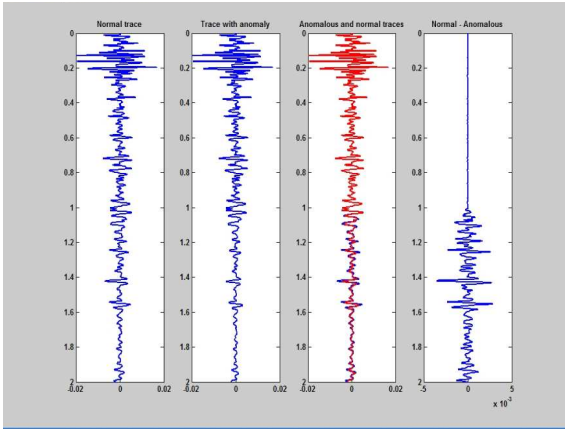

(b) Left–right: normal trace, anomalous trace, traces superimposed, difference of traces.

Figure 4.1: The seismic trace corresponding to the attenuation anomaly is nearly identical to the normal attenuation case.

4.3 Anomaly Detection Using Moments of Frequency

With the model (4.5) of seismic attenuation that we are using, it is clear that the amplitudes of higher frequency components attenuate more over the same depth than do lower frequency components. The net effect of this phenomenon is that there is a *red-shift* in the signal as it propagates through the earth. For example, in Figure 4.3 we show the amplitude spectrum of the source signal in blue, and the post-attenuation spectrum in red. A clear shift in the mean frequency is seen. The strategy we propose in this section is to look at the amplitude spectrum of the seismic trace over many overlapping windows in time, and look at the changes in the mean frequency of these spectra. These changes should correlate well with changes in attenuation.

With a given seismic data $s(t)$, we can take a windowed Fourier transform (e.g. the Gabor transform) to see the local spectral property of the data:

$$\hat{s}_g(t,\omega) = \int_{-\infty}^{\infty} s(\tau) g(t-\tau) e^{-i\omega\tau}\, d\tau, \tag{4.10}$$

where g is a Gaussian function used as a window. We can then compute the average with respect to the frequency to obtain the centroid frequency, $f_c(t)$, by the formula:

$$f_c(t) = \frac{\int \omega |\hat{s}_g(t,\omega)|\, d\omega}{\int |\hat{s}_g(t,\omega)|\, d\omega} \approx \frac{\sum_k \omega_k |\hat{s}_g(t,\omega_k)|}{\sum_k |\hat{s}_g(t,\omega_k)|}. \tag{4.11}$$

In a similar fashion, we could also compute other moments. During the workshop, we computed the second moment, and expect an amplification of the red-shift phenomenon.

$$f_s(t) = \frac{\int \omega^2 |\hat{s}_g(t,\omega)|\, d\omega}{\int |\hat{s}_g(t,\omega)|\, d\omega} \approx \frac{\sum_k \omega_k^2 |\hat{s}_g(t,\omega_k)|}{\sum_k |\hat{s}_g(t,\omega_k)|}. \tag{4.12}$$

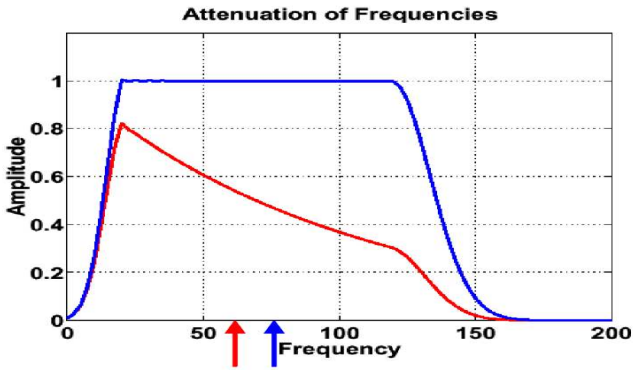

Figure 4.2: Shift in mean frequency: amplitude spectrum in red is for signal after attenuation.

Since we can expect a sudden decay of overall frequency amplitudes when sharp anomalies occur, we may observe lower values of $f_c(t)$ at the abnormality. We test this hypothesis by examining both the synthetic data from Section 4.2, as well as real data provided by Prof. Margrave. On both sets of data, we look at the trends in f_c and the second moment f_s.

4.3.1 Simulation with Synthetic Data

We tested the attributes f_c, f_s as predictors of the onset of attenuation anomalies on the synthetic data described in Section 4.2.3. In Figure 4.3 the centroidal frequency f_c of the anomalously attenuated signal is decreasing faster after $t = 1$ than that of the normal signal, acting as a good indicator of the abnormality.

In Figure 4.4 we show the variation in the second moment f_s for the seismic traces in the normal (blue) and anomalous (red) case. We also check the robustness of this attribute to noise; for very low levels of noise, the second moment is still a good predictor of the onset of the instability. As the noise increases, the amplitude spectra become too polluted in the high frequency regime to yield accurate predictions.

In real situations one does not have reference data to compare with. Thus, if we use these attributes, there should be intrinsic changes in the values of these attributes which allows us to identify anomalous behaviour.

Through many experiments we initially suggested that the graph of the centroid frequency f_c as a function of depth becomes concave near the onset of an anomaly. Unfortunately we found that while this concavity necessarily happens near abnormality, it also happens even in normal regions, which makes the criteria rather useless. Nevertheless we will see that the centroid frequency still acts as a good indicator for abnormality in the next section.

4.3.2 Simulation with Real Data

To test the ability of the centroidal frequency techniques to find attenuation anomalies in real data, we used two data sets provided by Prof. Margrave. These were seismic profiles taken at two geographical

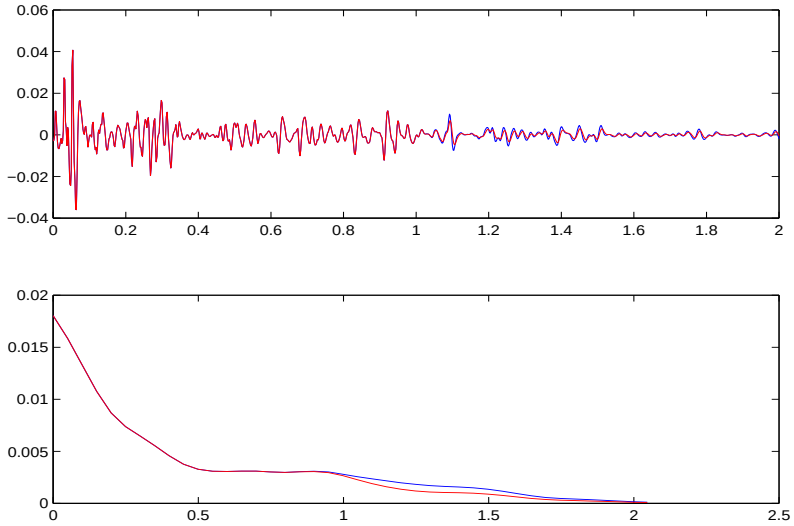

Figure 4.3: Above: Synthetic signals. Below: Centroid frequencies f_c for both traces over many windows. Note f_c values for "normal trace" are greater than the "anomalous trace".

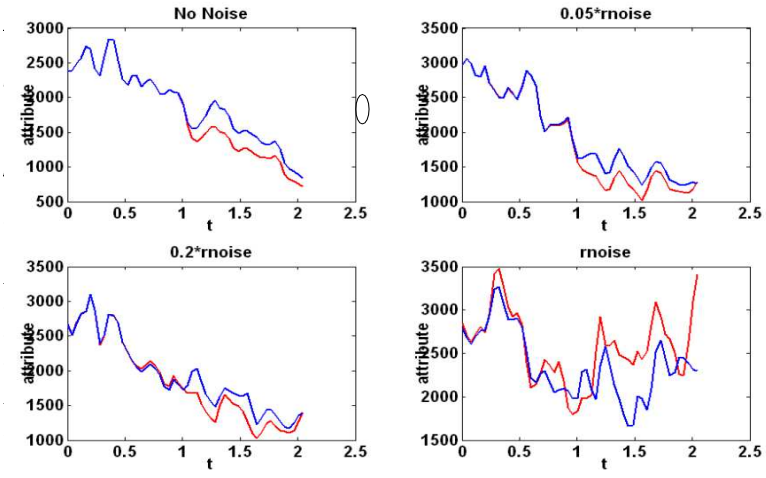

Figure 4.4: Synthetic signals and the second moment of frequency. Adding noise renders the detection of the anomaly less robust.

locations: Pike Peak and Blackfoot, respectively. In Figure 4.5 we see the *seismic cross sections* associated with the two data sets: in each, many source-receiver pairs were located along a horizontal line, and data was collected over a period of time. In these figures, the surface of the earth is on top; the y axis indicates depth (equivalently time of travel of the signal).

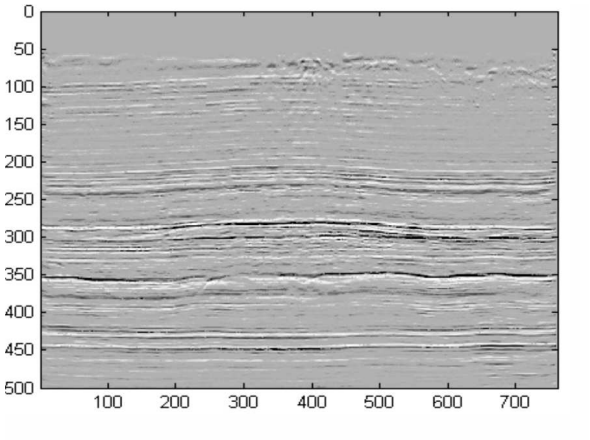

(a) Pikes Peak: anomaly at depth 350, location x=400.

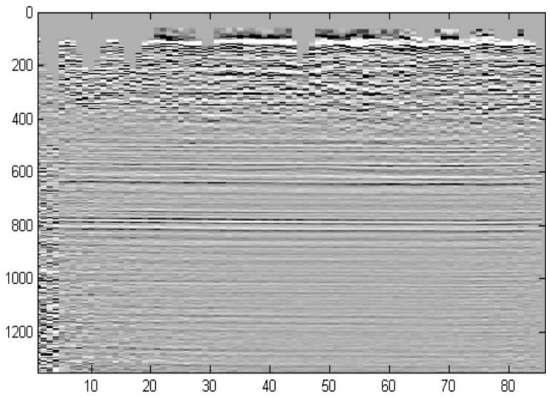

(b) Blackfoot reservoir: anomaly at depth t=600, location x=40-50.

Figure 4.5: Actual seismic traces: Pikes Peak and Blackfoot.

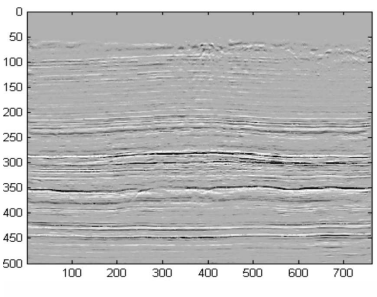

(a) Pikes Peak: actual trace.

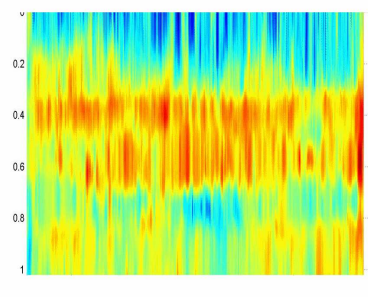

(b) Centroidal frequencies f_c.

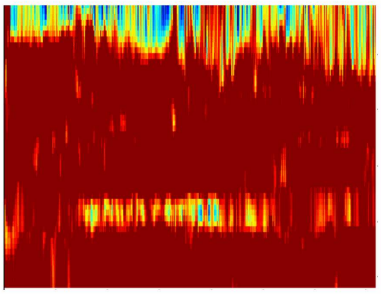

(c) Second moments f_s.

Figure 4.6: The Pike Peaks data set: the actual section, and the attribute-derived sections. Both f_c and f_s predict the anomaly at depth 350 well.

In Figures 4.6(b) and 4.7(b), the red indicate that the centroidal frequency f_c over a given window is high, and blue indicates a low f_c. In Figure 4.6(b), one sees a region of sudden decay of f_c at depth approximately 350, and location 400. In Figure 4.7(b), one can clearly see a region in yellow (lower f_c at depth 600, location $45 - 50$, identifying the presence of an attenuation anomaly. This region corresponds well with a known gas reservoir.

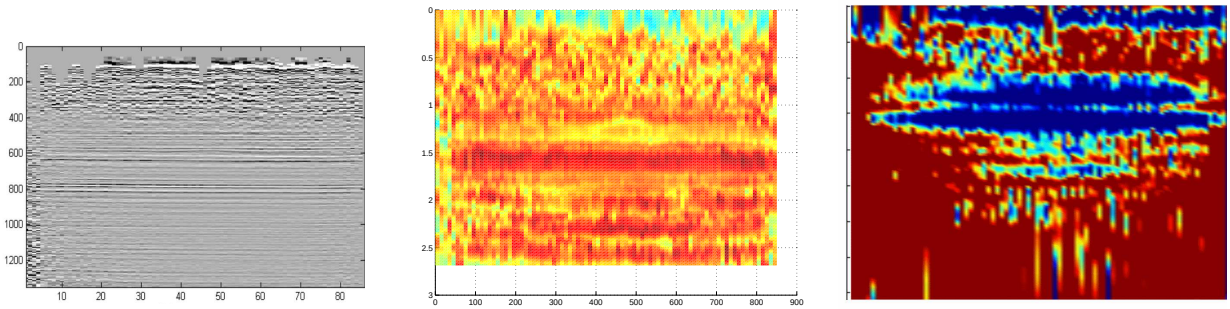

(a) Blackfoot: actual trace. (b) Centroidal frequencies f_c. (c) Second moments f_s.

Figure 4.7: The Blackfoot data set: the actual section, and the attribute-derived sections. f_c captures anomaly at $t = 600$, f_s less sharply resolved.

In Figures 4.6(c) and 4.7(c), regions of large deviation from the mean f_s are highlighted in blue. Again, in Figure 4.6(c) one sees an anomaly at depth 350. The width of this region appears larger than in 4.6(b); it would be interesting to cross-check this with any known geological features there. Likewise, Figure 4.7(c) picks out a wide band of anomalous attenuation at depth 300, an a narrower, more localized band at depth 600.

4.4 Wavelet-Based Techniques

In this section, we started with the assumption that the Fourier transform of the seismic trace s is proportional to the Fourier transform of the reflectivity r, where the proportionality factor is positive and contains information on the source signal and the attenuation factor. In other words, we can say

$$\hat{s}(\omega) \propto \hat{r}(\omega) e^{-A(\omega,t)}.$$

Here A can be parametrized by Q, and has the form $A(\omega, t) = \int_0^t a(\omega, u)\, du$. By taking the Fourier transform, we turn the convolution in the time domain into a multiplication in the Fourier domain.

The basic idea is to remove the reflectivity r in order to be left only with the information on the attenuation and the source function. The deconvolution being a hard problem, we would like to rewrite the problem in a much easier way so that we could separate the reflectivity from the other information. So after taking the Fourier transform, we take logarithms to transform the multiplication into a summation:

$$\log(|\hat{s}|) = -A(\omega, t) + \log(|\hat{r}|).$$

Then we can consider the data d as a sum of a model $m = -A(\omega, t)$ (including attenuation and the source signature) and coloured noise $n = \log(|\hat{r}|)$ (reflectivity). We have now a denoising problem in the *log-Fourier domain*.

4.4.1 Denoising Using Wavelets

In order to denoise the data, we use wavelet thresholding (we used only hard thresholding). Practically, we took a Windowed Fourier transform of the seismic traces, the result of which depends on both time and frequency. Then we took the logarithm of its absolute value.

The smoothness properties are different in the time and the frequency direction, so we exploited that by taking a different wavelet transform along each direction. Along the time direction, the traces should be piecewise constant as it should be constant where the Q is constant and only change when Q changes. On the other hand, the traces should be relatively smooth along the frequency direction. It is important to choose the right wavelet to represent our signal.

So the denoising method is as follows:

1. We take a 2D wavelet transform
2. We threshold the coefficients according the noise level (prior information on the statistics of the reflectivity)
3. We take a 2D inverse wavelet transform. The result is the denoised data which should scale like the amplitude $-A(\omega, t)$.

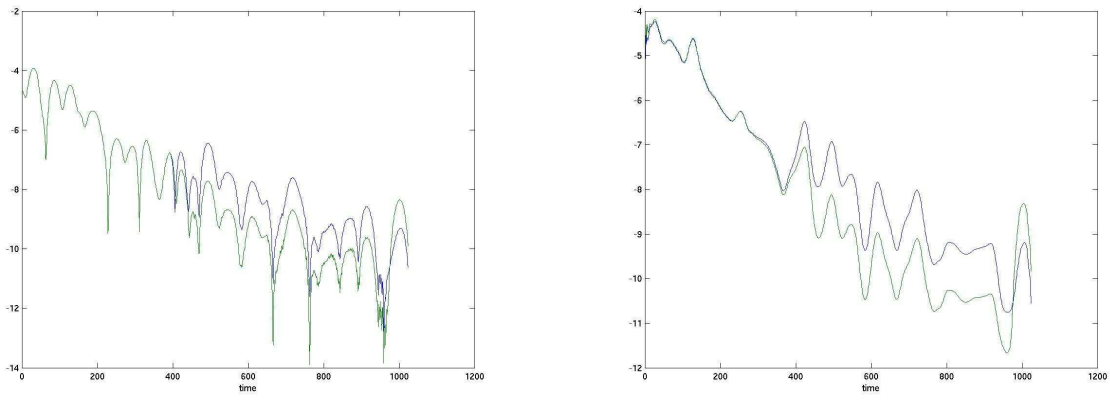

(a) Normal (blue) and anomalous (green) traces in the *log-Fourier domain* before denoising.

(b) With thresholding.

Figure 4.8: Normal (blue) and anomalous (green) traces in the *log-Fourier domain*, before and after denoising.

We apply this technique to the synthetic data as generated in Section 4.2.3. We can see from the two figures in Figure 4.8 that the difference between the normal and anomalous traces is enhanced by the thresholding because we took most of the reflectivity contribution out which is mostly the oscillatory part.

4.4.2 Denoising Using a Minimization Technique

Recall that we are seeking to locate $-A(\omega, t)$ from noisy data d, where

$$d = \log(|\hat{s}|) = -A(\omega, t) + \log(\hat{r}) = m + n.$$

We have already discussed a wavelet-based denoising strategy above. Another possible means of removing the noise from the data is to solve a minimization problem

$$\min_m \frac{1}{2}\|C_n^{-1/2}(d - m)\|_2^2$$

where C_n is the covariance matrix of the noise $C_n = E[nn^T]$. We can use a wavelet transform W to convert the minimization problem into

$$\min_{\tilde{m}} \frac{1}{2}\|\Gamma^{-1}(\tilde{d} - \tilde{m})\|_2^2 + \lambda\|\tilde{m}\|_p, \qquad \text{where } \tilde{d} := Wd,\ \ \tilde{m} = Wm,\ \ \tilde{n} = Wn,\ \ E[\tilde{n}\tilde{n}^T] = \Gamma^2.$$

The noise thresholding used is called hard or soft, depending on whether $p = 1$ or 2 respectively. Solving the minimization problem and subsequently inverting allows us to reconstruct an approximation to m.

4.5 Extension of the Wiener Technique

The relation between the measurement $s(t)$ and the initial wave $w(t)$ can be written in form of a modified convolution, i.e.

$$s(t) = w(t) * a \odot r(t) := \int w_\alpha(\tau, t - \tau) r(\tau) d\tau. \tag{4.13}$$

The kernel w_α contains the attenuation function $Q(t)$, which we eventually would like to determine:

$$w_\alpha(u, v) = \int \hat{w}(\eta)\alpha(u, \eta)\mathrm{e}^{i\eta v} d\eta, \tag{4.14}$$

$$\alpha(u, \eta) = \exp\left(-\frac{u\,\mathrm{sgn}(\eta)\eta}{2Q(u)} + i\frac{u\,\mathrm{sgn}(\eta)\mathcal{H}(\eta)}{2Q(u)}\right). \tag{4.15}$$

Here, $\hat{w}$ denotes the Fourier transform of w and $\mathcal{H}$ the Hilbert transform. In the case without attenuation, this expression reduces to $s = w * r$. Therefore, we can write for small attenuation, corresponding to large Q, a Taylor expansion of the kernel α and use the first nontrivial terms in this expansion in order to derive higher order corrections to the relation $s = w * r$. For $\alpha(u, \eta)$ we find

$$\alpha(u, \eta) = \sum_{k=0}^{\infty} \frac{1}{k!}\left(\frac{u}{2Q(u)}\right)^k \kappa(\eta)^k \tag{4.16}$$

with the abbreviation

$$\kappa(\eta) = -\mathrm{sgn}(\eta)\eta + i\mathrm{sgn}(\eta)\mathcal{H}(\eta). \tag{4.17}$$

In the above expression, the arguments u and η are decoupled in the sense that we can perform the integration with respect to η in the expression (4.14) for w_α. Thus we obtain for w_α the expansion

$$w_\alpha(u,v) = w(v) + \frac{u}{2Q(u)}J_1(v) + \frac{1}{2}\left(\frac{u}{2Q(u)}\right)^2 J_2(v) + \dots \tag{4.18}$$

where the $J_n(v)$ depend on the initial wave w by

$$J_n(v) = \int \hat{w}(\eta)\kappa^n(\eta)\mathrm{e}^{i\eta v}d\eta. \tag{4.19}$$

Now we are ready to write the higher order correction terms to the relation between the initial wave w and our measurement s:

$$s = w * r + \left(\frac{tr(t)}{2Q(t)}\right) * J_1 + \frac{1}{2}\left[\left(\frac{t}{2Q(t)}\right)^2 r(t)\right] * J_2 + \dots. \tag{4.20}$$

The basic problem of determining Q lies in the fact that we don't have complete knowledge of either r or w. We have, however, information about the statistical properties of r. A very realistic assumption is that the autocorrelation function of r is a delta function. Writing $\tilde{f}(t) = f(-t)$ this means that

$$r * \tilde{r} = \delta(t). \tag{4.21}$$

Therefore, looking at the autocorrelation of s, we can try to eliminate first the terms involving r in order to reduce our problem significantly. Let us assume for sake of simplicity first that Q is a constant. Then, our expansion reduces to

$$s * \tilde{s} = w * r * \tilde{w} * \tilde{r} + \frac{1}{2Q}(tr) * J_1 * \tilde{w} * \tilde{r} - \frac{1}{2Q}(t\tilde{r}) * \tilde{J}_1 * w * r + \dots. \tag{4.22}$$

Assuming now that all convolutions of r can be approximated by delta functions

$$(t^n r) * \tilde{r} = \beta_n \delta(t) \tag{4.23}$$

we see that, in the above expression, all dependency of r vanishes and we obtain an equation that *only* depends on w and Q but not on r

$$s * \tilde{s} = w * \tilde{w} + \frac{\beta_1}{2Q}J_1 * \tilde{w} - \frac{\beta_1}{2Q}w * \tilde{J}_1 + \dots. \tag{4.24}$$

This result reduces for $Q \to \infty$ to the classical Wiener technique, meaning that then the initial wave w can be found by the power spectrum of s and causality assumptions. Equations (4.24) incorporates the influence of Q in form of higher order correction terms.
There are two major directions for future research on the basis of this result:

1. Approximation of w by a Gabor transform using the first part of the measured signal s and finding Q through the above formula with the estimated w.

2. Use the above result in order to reduce the space for possible candidate functions for w and Q in combination with the other developed techniques.

4.6 Conclusions and Future Work

During the course of the workshop, our team did not conclusively solve the severely ill-posed problem of computing seismic attenuation from given surface seismic trace data. However, we learnt about several techniques currently being used, and began studying some other possibilities. Our efforts can be summarized by:

1. an investigation of the utility and robustness of frequency-related attributes as predictors of anomalous attenuation. These efforts are closely related to those of [6]. Under this heading, we investigated two attributes: the centroidal frequency of a windowed seismic trace, and the second moment of frequency;

2. using wavelet-based techniques to remove reflectivity information from the trace (denoising) and subsequently extract attenuation information

3. an extension of the Wiener technique to the case with attenuation.

In addition to pursuing these further (particularly through numerical implementation of the two latter strategies), we would also like to investigate the use of statistical and linear-algebra techniques to retrieve information about attenuation anomalies.

Bibliography

[1] Hedlin, K. Mewhort, L. & Margrave, G. (2001). *Delineation of steam flood using seismic attenuation*. Expanded Abstracts, 71st. Annual International Meeting, Society of Exploration Geophysicists, pp. 1572–1575.

[2] Kumar, G. Batzle, M. & Hofmann, R. (2003). *Effects of fluids on the attenuation of elastic waves*. Expanded Abstracts, 73st. Annual International Meeting, Society of Exploration Geophysicists, pp. 1592–1595.

[3] Pride, S. R. & Berryman, J. G. (2003). *Linear dynamics of double-porosity dual-permeability materials I. Governing equations and acoustic attenuation*. Physics Review E, 68, 36603.

[4] Pride, S. R. & Berryman, J. G. (2003). *Linear dynamics of double-porosity dual-permeability materials II. Fluid transport equations*. Physics Review E, 68, 36604.

[5] Pride, S. R., Harris, J. et al. (2003). *Permeability dependence of seismic amplitudes*. The Leading Edge, 22(6), pp. 518–525.

[6] Quan, Y. & Harris, J. M. (1997). *Seismic attenuation tomography using the frequency shift method*. Geophysics, 62(3), pp. 895–905.

[7] Winkler, K. W. & Nur, A. (1982). *Seismic attenuation: Effects of pore fluids and frictional-sliding*. Geophysics, 47(1), pp. 1–15.